Nuclear Instruments and Methods in Physics Research A 772 (2015) 76–82

Contents lists available at ScienceDirect

Nuclear Instruments and Methods in Physics Research A

journal homepage: www.elsevier.com/locate/nima

Understanding avalanches in a Micromegas from single-electron response measurement

T. Zerguerras [a,*], B. Genolini [a], F. Kuger [b,c], M. Josselin [a], A. Maroni [a], T. Nguyen-Trung [a], J. Pouthas [a,1], P. Rosier [a], Ö. Şahin [d], D. Suzuki [a], R. Veenhof [d,e]

[a] Institut de Physique Nucléaire (UMR 8608), CNRS/IN2P3-Université Paris-Sud, F-91406 Orsay Cedex, France
[b] University of Würzburg, 97070 Würzburg, Germany
[c] CERN, Geneva, Switzerland
[d] Department of Physics, Uludağ University, 16059 Bursa, Turkey
[e] RD51 Collaboration, CERN, Geneva, Switzerland

ARTICLE INFO

Article history:
Received 4 July 2014
Received in revised form
19 September 2014
Accepted 5 November 2014
Available online 13 November 2014

Keywords:
Gaseous detectors
Micromegas
Single-electron response
Avalanche charge fluctuations
Magboltz Monte-Carlo model

ABSTRACT

Avalanche fluctuations set a limit to the energy and position resolutions that can be reached by gaseous detectors. This paper presents a method based on a laser test-bench to measure the absolute gain and the relative gain variance of a Micro-Pattern Gaseous Detector from its single-electron response. A Micromegas detector was operated with three binary gas mixtures, composed of 5% isobutane as a quencher, with argon, neon or helium, at atmospheric pressure. The anode signals were read out by low-noise, high-gain Cremat CR-110 charge preamplifiers to enable single-electron detection down to gain of 5×10^3 for the first time. The argon mixture shows the lowest gain at a given amplification field together with the lowest breakdown limit, which is at a gain of 2×10^4 an order of magnitude lower than that of neon or helium. For each gas, the relative gain variance f is almost unchanged in the range of amplification field studied. It was found that f is twice higher ($f\sim 0.6$) in argon than in the two other mixtures. This hierarchy of gain and relative gain variance agrees with predictions of analytic models, based on gas ionisation yields, and a Monte-Carlo model included in the simulation software Magboltz version 10.1.

1. Introduction

For more than a decade, micro-pattern gaseous detectors (MPGDs), such as the GEM [1] and the Micromegas [2], have proven to be valuable tools for high-energy physics thanks to their good energy, time and position resolutions, their high rate capability, their low spark rate and their ability to limit ion backflow. MPGDs are found in virtually all high energy physics experiments [3–6]. They also appear as most promising technologies for the LHC instrumentation upgrade [7–9] and are considered as part of the detection system associated to the future International Linear Collider (ILC) facility [10].

MPGD devices are also growing in importance in modern nuclear physics, where new generations of radioactive-isotope beam facilities [11–14] will soon be extending horizons of spectroscopic studies on short-lived nuclei. A new generation of MPGD enables a unique access to nuclear reactions at low energies or rare decay processes. A time-projection chamber (TPC) using a stack of four GEM foils realised direct measurements of two-proton decay of ^{45}Fe, a very rare mode of radioactivity [15]. Active reaction targets for radioactive-beam reactions are another example of applications that are attracting much of attention [16–18]. These devices are based on TPC technology, where the tracking gas is used simultaneously as the target of nuclear reactions. The reaction vertex and energy deposition of particles, of which the uncertainty usually leads to critical deterioration of resolutions, can be directly and precisely measured. In pursuit of better resolution and higher luminosity, active targets using MPGD devices such as ACTAR TPC [19], AT-TPC [20], or CNS-TPC [21] are currently under development.

This paper looks into the multiplication process in a Micromegas detector, with particular focus on the avalanche charge fluctuations which limit the energy [22] and position [23] resolutions. Although experimental data quantifying these fluctuations are critical for gaseous detectors simulation programmes, they are rather scarce in tables and literature. This paper proposes a method ideally suited to get such data. It is based on measurements of the single-electron response (SER) of a Micromegas detector, operated with helium, neon and argon gas mixtures with

* Corresponding author. Tel.: +33 1 69 15 64 42; fax: +33 1 69 15 50 01.
E-mail address: zerguer@ipno.in2p3.fr (T. Zerguerras).
[1] Present address: Laboratoire de Physique Corpusculaire, ENSICAEN, Bvd Maréchal Juin, 14050 Caen, France.

http://dx.doi.org/10.1016/j.nima.2014.11.014
0168-9002/

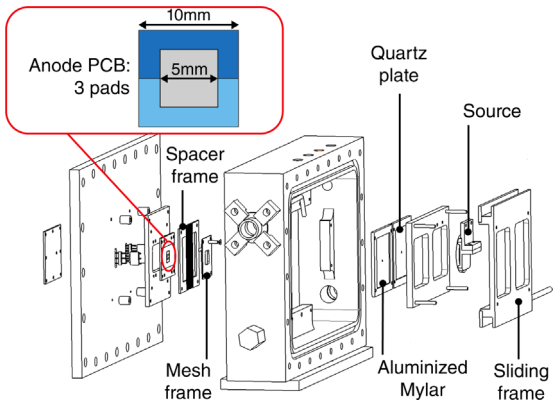

Fig. 1. Exploded view of the detector.

isobutane. Compared to the traditional use of a radioactive source or a charged particles beam, this method provides a direct measurement of the absolute gain and the relative gain variance but requires an optimised test-bench, in terms of detector mechanics and electronics signal-to-noise ratio, to enable single electron detection in a wide range of electric field, down to gains as low as a few 10^3.

Section 2 describes the experimental method and the setup. Section 3 reports on the peculiarities of the avalanche process in the used gas mixtures. Results and interpretations of SER measurements, including gain curves and relative gain variance, are given in Section 4.

2. Experimental method

The set-up relies on a previously used optical test-bench [24], that consists of a 337-nm pulsed laser, model VSL-337 from Spectra-Physics [25], a telescope collimating the laser beam, a periscope adjusting its height and a 60-mm focal length triplet, giving a spot size smaller than 100 μm. The purposes of the present measurements call for a new detector, shown in Fig. 1, with an improved design compared to that used in Ref. [24], including a simplified anode pad plane and readout electronics with an improved signal-to-noise ratio to lower the single-electron detection threshold.

The Micromegas drift electrode is divided into a stretched aluminized Mylar® foil for measurements with an ^{55}Fe source and a thin quartz plate with a 0.5-nm thick nickel–chromium layer for operation with the laser. The drift electrode is mounted on a sliding frame which allows us to place either part of the electrode in front of the Micromegas mesh. The ^{55}Fe source is mounted on the sliding frame and faces the Mylar® foil. The mesh foil of the Micromegas is a 333 lines-per-inch electroformed nickel micromesh, manufactured by Buckbee-Mears and supplied by Industrial Netting [26], with an optical transparency of 70%. The Micromegas has an active area of 10×10 mm^2 and was installed 3.2 mm from the drift electrode. The gap between the mesh and the anode is defined by 160-μm diameter stretched nylon fishing lines at 2 mm intervals. The anode printed-circuit board (PCB) is divided in a 5×5 mm^2 square pad and two adjacent bracket-shape pads. The Micromegas structure with the ^{55}Fe source is enclosed in a vessel equipped with a quartz entrance window (not shown in Fig. 1) which transmits the laser-light unattenuated. The vessel is mounted on three 1-μm precision motors to move the detector relative to the laser beam.

In order to lower the charge threshold for SER measurements, the signal-to-noise ratio of the pads readout electronics was enhanced by replacing the Gassiplex chips [27] used in Ref. [24] by CR-110 charge preamplifiers manufactured by Cremat [28]. This chip achieves high gain (1.4 V/pC) with a much lower noise level (200 e$^-$ RMS) than the Gassiplex. The CR-110 chips were mounted on a board enclosed in a metallic box connected to the anode pads on the rear side of the vessel. The box was also equipped with three test-inputs to inject a generator pulse signal through a 1 pF high-precision capacitance for charge calibration and electronics noise measurement of each channel. When connected to the detector, the electronics noise was increased to 380 e$^-$ RMS due to the detector capacitance. However, this is still a factor of 5 lower than in the previous set-up using Gassiplex chips.

Each preamplifier output feeds a 16-channel CAEN N568B spectroscopy amplifier [29] with a shaping time set at 3 μs. The N568B module outputs both slow and fast signals. The slow signals were digitised by an 11-bit CAMAC-standard peak-sensing ADC module AD811F. The data acquisition was triggered by the fast signal of the central pad when using the ^{55}Fe source and the events with full energy deposition in the central pad were selected in the analysis of the ^{55}Fe data.

The single-electron regime is achieved following the method described in Ref. [24]: the pulsed laser is focused on the metallic layer of the quartz plate to generate a signal on the central pad only. Then, the laser light intensity is attenuated with calibrated neutral density filters to a regime where the probability of producing one electron is much greater than the probability of giving more than one. In this new set-up, the laser light was attenuated by a factor of 200 and fewer than 5% of the triggered events have a non-zero signal (charge greater than 2×10^3 electrons, which is 5 times the RMS noise). Among these non-zero signals, the probability of producing more than one electron is lower than 0.25%. In single-electron mode, the trigger was generated using a split laser light that was routed by an optical fiber to a Photonis XP2282B photomultiplier [30]. The charge of the anode signal from the photomultiplier was recorded in a standard CAMAC QDC module (model Lecroy AD2249A) to monitor the laser light fluctuations. The Micromegas drift field is kept at 900 V/cm.

The three gas mixtures were of 95% of argon, neon or helium, and 5% isobutane (iC_4H_{10}). The Air Liquide company [31] supplied the gases, with a purity better than 99.999% for the rare gases and 99.5% for isobutane, which were then mixed according to the aforementioned proportions by adjusting the gas flows using Brooks [32] digital flowmeters. A gas regulation system is connected at the gas input and output to empty the vessel, and maintain a stable flow and a constant pressure of 748 Torrs. All measurements were conducted in a controlled-temperature room at 293 ± 0.5 K.

Isobutane is an efficient quenching gas due to its high photo-absorption cross-section [33]. The argon-based mixture is widely used for characterising Micromegas detectors and a typical ^{55}Fe spectrum measured with the present set-up is shown in Fig. 2, where the main 5.9 keV and the 2.9 keV escape peaks are both visible. The energy resolution obtained for the 5.9 keV peak is 20% FWHM. Neon mixtures are light and feature high gains with low spark rates [34]. Performances of Micromegas in helium-based mixture are important for the active target application as helium nuclei are widely used targets of nuclear reactions.

To avoid any damage on the Cremat chips, the mesh voltage where Micromegas was safely operated without discharge was determined before starting any measurements. During this preparation, the preamplifiers were dismounted and the anode pads were directly grounded. The mesh voltage was increased up to observe a first spark and the maximum operation voltage was set 10 V below the measured discharge threshold. The corresponding electric field of amplification ranged from 24 to 35 kV/cm.

3. Avalanche processes

This section describes the electron avalanche mechanism in the gas mixtures used for the present study. It also reviews the microscopic avalanche simulation that we developed and that is compared with experimental results in Section 4.

3.1. Excitation and ionisation

Electrons collide elastically and inelastically with gas molecules when they travel from the drift electrode to the mesh. Between the mesh and the anode, the electrons reach energies at which additional processes such as attachment, excitation and ionisation become available. As a result, an avalanche develops.

Multiplication is in part due to direct ionisation. But excited noble gas atoms may have sufficient excess energy to ionise quencher molecules in a process known as the Penning transfer [35,36]. Isobutane has a particulary low ionisation potential (10.67 eV) and all excited states of argon, neon and helium are energetically eligible for collisional transfer [37,38]. Although excitation cross-sections are generally smaller than ionisation cross-sections, indirect ionisation via collisional transfer is allowed at lower energies. Excited noble gas atoms are therefore abundantly produced and the Penning transfer is a significant contribution to the gas gain.

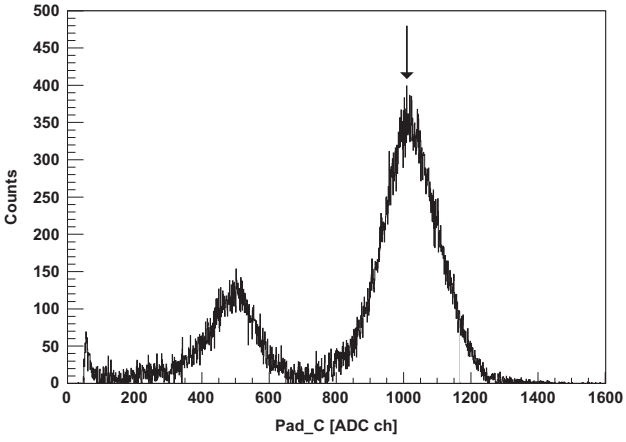

Fig. 2. ^{55}Fe spectrum measured with Ar 95% iC_4H_{10} 5% at a drift field of 900 V/cm and an amplification field of 28 kV/cm. The arrow indicates the full-energy absorption peak of 5.9 keV X-ray.

The left panel of Fig. 3 shows that the direct ionisation rate of isobutane is one order of magnitude larger than the ionisation rate of noble atoms in the helium and neon mixtures. But the direct ionisation rate of isobutane is comparable to that of argon in the argon-based mixture. The total ionisation rate of isobutane and noble gas are compared with the excitation rate of noble atoms in the right panel of Fig. 3. The direct ionisation rate is much higher than the excitation rate in the helium and neon mixtures, while excitation dominates direct ionisation in the argon mixture. Unless the argon mixture displays a particularly strong Penning effect, part of the excitation energy will be lost causing larger gain fluctuations than in the other mixtures [39]. All ionisation rates in this study were calculated using Magboltz 10.1 [40].

3.2. Avalanche statistics

Avalanche formation is a stochastic process since the path length between successive interactions, and accordingly the electron energy, varies. In most collision, several scattering mechanisms are allowed (elastic, inelastic, attachment, excitation, and

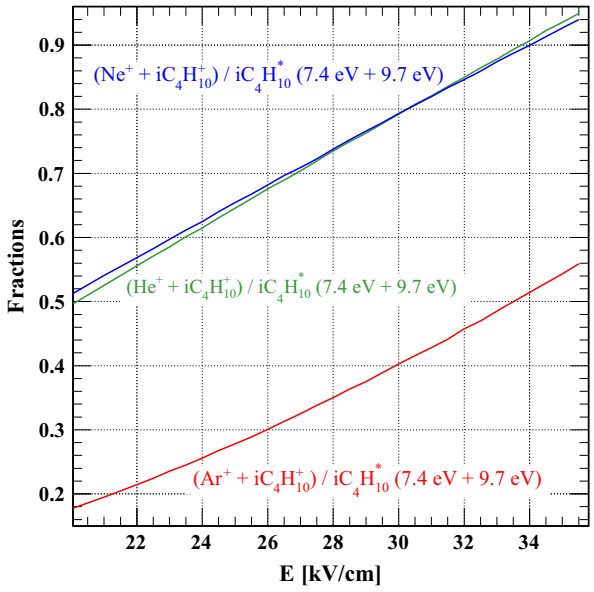

Fig. 4. Ratio of total ionisation rate to the rate of excitation to the state at 7.4 and 9.7 eV in isobutane, calculated with Magboltz 10.1.

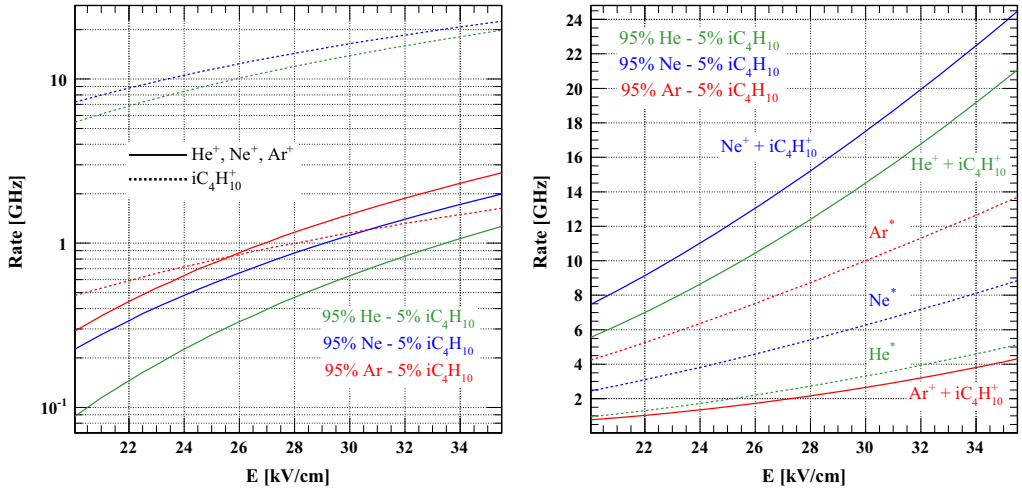

Fig. 3. (Left) Direct ionisation rate of noble gas atoms (solid lines) and iC_4H_{10} molecule (dashed lines). (Right) Total rate of direct ionisation of isobutane and noble gases (solid lines) and total rate of excitation of nobles gases (dashed lines). Calculations were made using Magboltz 10.1.

ionisation) with likelihoods that depend on the electron energy, e.g. an electron with sufficient energy to ionise a gas atom could still lose its energy by exciting it. Unless the excitation energy is transformed into ionisation, the excitation energy is lost, leading to increased avalanche charge fluctuations. Consequently, gas mixtures with a high ionisation over excitation ratio have narrower avalanche charge distributions. According to Magboltz 10.1 calculations presented in Fig. 4, the argon mixture appears thus least favourable.

Avalanche charge fluctuations depend on the gas mixture, the reduced electric field E/p (ratio of the electric field E to the pressure p), the electron initial momentum and the distance over which the avalanche is allowed to develop. At low E/p, the avalanche charge distribution is exponential according to the so-called Yule–Furry model. At higher E/p, many experimentally measured SER show a maximum [41–44]. Such distributions have a relative gain variance smaller than 1, which leads to better energy and position resolution [45].

Given the variety of processes which contribute to avalanche development, and considering that even Legler's simplified model [46] has no closed-form solution, the Monte-Carlo method is suited to simulate electron avalanches. It has the advantage of being reasonably efficient while taking all known effects into account. In the present study, we carried out a simulation by integrating Garfield++ [47] with Magboltz 10.1. In this simulation, processes such as excitation and ionisation of molecules, electron attachment and the Penning transfer were taken into account, while the feedback effect induced by de-excitation UV or avalanche ions was not. In particular, if an excited state is capable of the Penning transfer, a new electron is produced with a probability r_p, the Penning transfer rate, and is processed as another electron avalanche.

4. Results

SER spectra were measured for the three binary mixtures argon, neon and helium with 5% iC_4H_{10} as a function of amplification field E. During the measurements, the laser light fluctuations monitored with the PMT are of 3% standard deviation. Fig. 5 shows examples of charge distributions measured for argon (top), neon (middle) and helium (bottom) gas mixtures. The charge is given in number of electrons N_e where the conversion parameters from ADC counts were deduced from the pulse calibration (see Section 2). For the neon and helium-based mixtures, the SER has a maximum which is less pronounced for the argon-based mixture. The spectra were fitted by a so-called Polya distribution (SP fit) which is expressed as

$$P(N_e) = \frac{(1+\theta)^{1+\theta}}{\Gamma(1+\theta)} \left(\frac{N_e}{\overline{N_e}}\right)^{\theta} \exp\left[-(1+\theta)\frac{N_e}{\overline{N_e}}\right] \quad (1)$$

where $\overline{N_e}$ is the mean gain and θ the Polya parameter which gives the relative gain variance f:

$$f = \left(\frac{\sigma_{N_e}}{\overline{N_e}}\right)^2 = \frac{1}{1+\theta}. \quad (2)$$

At gains smaller than 10^4, the fit is biased by the pedestal distribution which overlaps with the bump of the SER distribution. In such a case, we included a Gaussian function in the fitting for the pedestal part (SGP fit).

For each amplification field, the gain and the relative gain variance were deduced from the fit, giving the data set shown in Figs. 6 and 7 respectively. It should be emphasised that using the

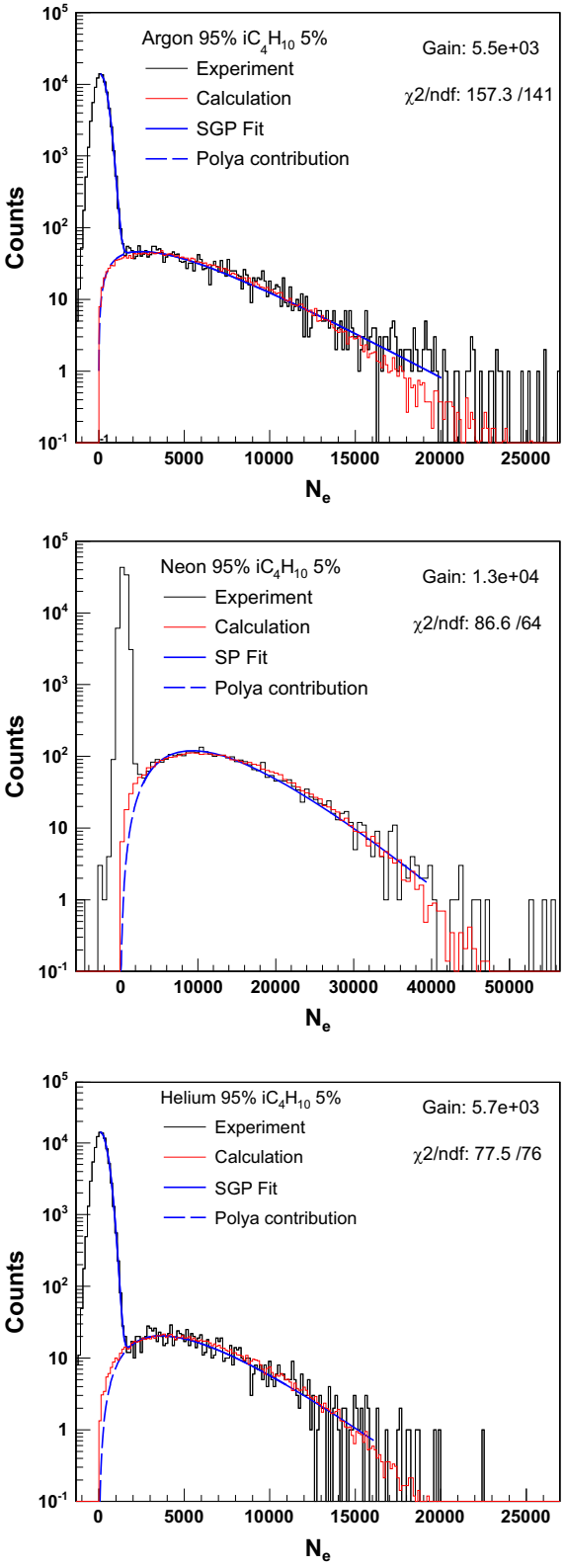

Fig. 5. Experimental SER spectra together with the best-fit curves (blue thick lines), the contribution of the Polya distribution (blue dashed lines), and the simulated SER distribution (red lines). The χ^2/ndf ratio refers to the fit likelihood. (Top) Argon 95% iC_4H_{10} 5%, $E=28.12$ kV/cm, SGP fit. (Middle) Neon 95% iC_4H_{10} 5%, $E=26.25$ kV/cm, SP fit. (Bottom) Helium 95% iC_4H_{10} 5%, $E=26.25$ kV/cm, SGP fit. (For interpretation of the references to colour in this figure caption, the reader is referred to the web version of this paper.)

new set-up enables us to measure these quantities down to a gain of 5×10^3, far lower than the limit (3×10^4) in the previous study [24]. It is also worth noting that this is the first measurement of relative gain variances at such a low gain for an argon–isobutane mixture.

The maximum gain before sparking is achieved with the neon-based mixture and is one order of magnitude higher than with argon. At a given E, the gain of the neon-based mixture is 7 times larger than in the argon-based mixture and 2 times larger than in the helium-based mixture. Thus, neon and helium are more suitable for applications where a wide range of gain is required.

As illustrated in Fig. 7, the relative gain variance f is almost unchanged over the measured range of electric field E in all three gas mixtures. The measurements for the neon mixture are in good agreement with our previous results in Ref. [24], where the SER of a Micromegas detector with the same amplification gap was measured in a narrower amplification field range (29–32 kV/cm). The relative gain variance of the helium mixture is very close to that of the neon (~0.35) whereas those of the argon mixture are twice higher (~0.6). This trend is in line with the conjecture from ionisation rate calculations presented in Section 3 and agrees with models, valid in uniform electric fields, which predict stronger avalanche fluctuations for a gas mixture with a low ionisation yield [39,48]. Moreover, the two mixtures with lower avalanche fluctuations have higher breakdown limits, and it is thus tempting to link the reduced discharge rate with the lower probability of larger spread avalanche charge distributions.

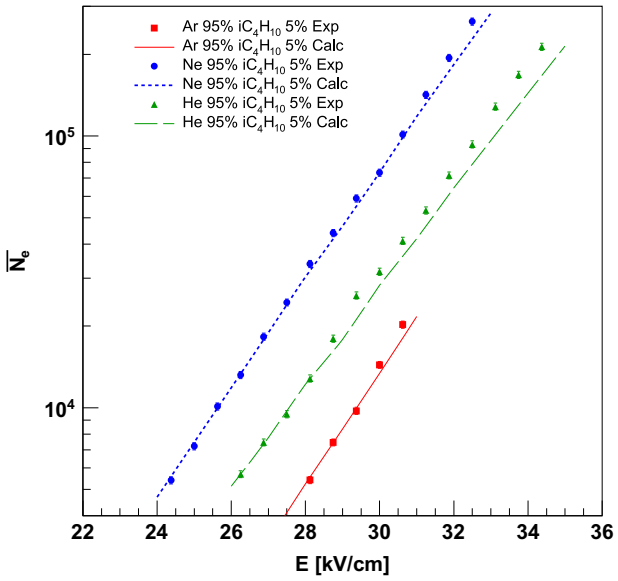

Fig. 6. Experimental mean gains $\overline{N_e}$ as a function of the amplification field E compared with the Monte-Carlo simulations for the argon, neon and helium gas mixtures.

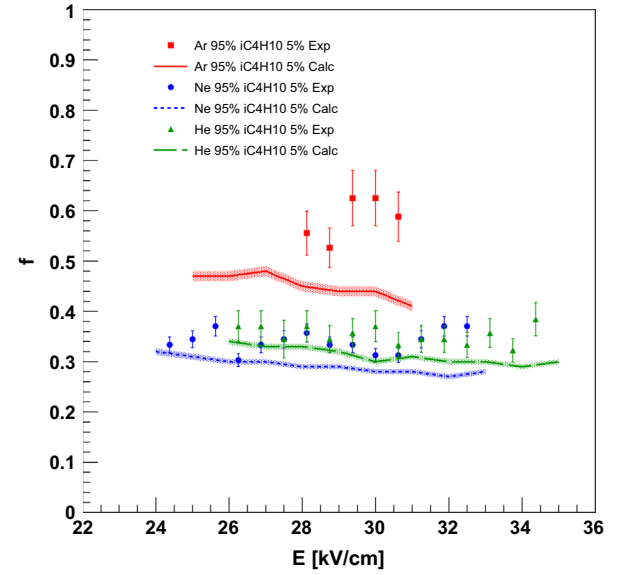

Fig. 7. Experimental relative gain variances f as a function of the amplification field E compared with the Monte-Carlo simulations for the argon, neon and helium gas mixtures. The shaded areas represent the statistical errors.

The Monte-Carlo simulation of avalanche processes, as described in Section 3, gives a quantitative interpretation of the experimental data. However, the technique is CPU-time consuming for large avalanches, and calculations using the CERN LXPLUS server requires approximately 200 h to generate 10^4 events at a gain above 10^5. Consequently, the full simulation was carried out only for the neon-based mixture at 20–26 kV/cm and for the helium and argon-based mixtures at 20–27 kV/cm. At higher electric-fields, the simulation was extrapolated in the second-half of the amplification gap, leading to a reduced calculation time of approximately 12 h for each voltage value.

The full avalanche development consists of a series of independent steps, where each single electron creates k electrons with a probability $p_i(k)$ during the i-th step. Assuming that equal conditions (gas parameters, step length and electric field) lead to equal probabilities during each step, the mean gain grows exponentially with the number of steps.

Calculations show that the mean gain $\overline{N_{\text{full}}}$ of full developed avalanche and the gain $\overline{N_{\text{half}}}$ for an avalanche developing over half the distance can be related introducing an exponent ξ:

$$\overline{N_{\text{full}}} = \overline{N_{\text{half}}}^{\xi}. \tag{3}$$

According to the geometry, one would expect $\xi=2$ but found 2.04 ± 0.01, 2.06 ± 0.01 and 2.07 ± 0.01 for the argon, neon and helium-based mixtures respectively. The reason is that, besides the conditions mentioned above, the amplification process depends on the initial energy of the electron, which is lower at the beginning of the avalanche formation compared to the electron energy after collisions in the amplification gap. In the first step, $p_i(k)$ is accordingly biased to lower values which leads to higher exponents ξ. This effect diminishes when the number of scatters the electron experiences increases in the 80 μm distance. It is thus less pronounced in argon compared to neon and helium because the electron mean free path is the shortest in this gas.

In homogeneous fields, the extrapolated relative variance can be derived by means of general statistics consideration according to [39]:

$$\left(\frac{\sigma_{N_{\text{full}}}}{\overline{N_{\text{full}}}}\right)^2 = \left(\frac{\sigma_{N_{\text{half}}}}{\overline{N_{\text{half}}}}\right)^2 \left(\frac{1-\left(\frac{1}{\overline{N_{\text{half}}}}\right)^{\xi}}{1-\frac{1}{\overline{N_{\text{half}}}}}\right). \tag{4}$$

The Penning transfer rate r_p was determined by repeating the simulation up to reproducing the experimental mean gain at an amplification field where feedback is assumed to be negligible, i.e. 28.12 kV/cm for the argon mixture and 26.25 kV/cm for the helium and neon-based mixtures. The Penning transfer so obtained is listed in Table 1. In the present simulation, r_p was assumed to be the same for all excited levels of each gas mixture. These excitation transfer rates together with ionisation rates presented in Fig. 3 help us in understanding the observed gain hierarchy since the neon mixture has both the highest ionisation yield and Penning transfer rate, whereas the r_p of the argon mixture does not compensate its lower ionisation yield.

Table 1
Excitation–ionisation transfer rate r_p extracted from the experimental gain curves. The errors are statistical.

Mixture	r_p
Ar iC_4H_{10} 5%	0.321 ± 0.003
Ne iC_4H_{10} 5%	0.482 ± 0.017
He iC_4H_{10} 5%	0.175 ± 0.025

SER spectra were simulated using the Penning transfer rates thus obtained. The results are compared to the experimental spectra in Fig. 5. Simulations agree with the experimental data of the neon and the helium mixtures, whereas the calculated spectrum of the argon-based mixture underestimates the spectrum tail. Fig. 7 shows such a discrepancy between calculated and experimental relative gain variance for this gas mixture. It can be explained by the absence of feedback in the model. When the electric field approaches the breakdown limit, the probability of secondary avalanches, either by ion backflow or UV photons, increases. While secondary avalanches increase the charge fluctuations in electron avalanches, these processes were not incorporated in the present simulation. For the three mixtures, calculations predict a slowly decreasing relative gain variance when the electric field increases whereas such a trend is not clear from the experimental data. Nevertheless, the contribution of feedback in the neon and helium mixtures is significant above 30 kV/cm. Another effect of feedback is observed in the mean gains in Fig. 6, where the difference between the calculated and experimental curves slopes increases above 30 kV/cm and can be due to secondary avalanches.

The Monte-Carlo model reproduces the gas mixture hierarchy and is consistent with the analytic models described in Section 3, since the argon mixture has the lowest ionisation yield and the poorest performances in terms of avalanche charge fluctuations and breakdown limit. For helium and neon, the Monte-Carlo model predicts gain and relative gain variances for electric fields up to 30 kV/cm despite its approximations.

5. Conclusion

A Micromegas detector with a 160-μm thick amplification gap was equipped with low-noise (380 e^- RMS when connected to the detector) Cremat charge preamplifiers. The detector was mounted on a laser test-bench and operated with three binary gas mixtures (argon, neon, or helium with 5% isobutane) to measure the single-electron response (SER) down to a gain of $\sim 5 \times 10^3$, which enabled us to study avalanche charge fluctuations of these gas mixtures for the first time at such low gains in a Micromegas detector. The mean gain and the relative gain variance were deduced from a fit using a Polya distribution. The argon mixture showed the lowest gain (7 times lower than neon for the same electric field), a relative gain variance ($\simeq 0.6$) almost twice larger than the two other mixtures and the lowest breakdown limit. Experimental results are consistent with analytical models predicting larger avalanche charge fluctuations for gas mixtures with lower ionisation rates. A Monte-Carlo simulation was carried out and its results were compared to the experimental data. The simulated mean gain agrees with the data at low electric fields, while it increasingly underestimates the gain at fields above 30 kV/cm. The relative gain variance was well reproduced for the neon and helium mixtures, while it was underestimated for the argon mixture. These discrepancies can be explained by a stronger feedback contribution, which is not included in the model.

Acknowledgments

The authors thank C. Thenault, M. Imre and L. Séminor, of the Institut de Physique Nucléaire (Orsay, France), who assembled the detector and H. Schindler of CERN (Geneva, Switzerland), for fruitful discussions on Magboltz.

References

[1] F. Sauli, Nuclear Instruments and Methods in Physics Research Section A 386 (1997) 531. http://dx.doi.org/10.1016/S0168-9002(96)01172-2.
[2] Y. Giomataris, et al., Nuclear Instruments and Methods in Physics Research Section A 376 (1996) 29. http://dx.doi.org/10.1016/0168-9002(96)00175-1.
[3] B. Ketzer, Nuclear Instruments and Methods in Physics Research Section A 494 (2002) 142. http://dx.doi.org/10.1016/S0168-9002(02)01457-2.
[4] M. Alfonsi, et al., Nuclear Instruments and Methods in Physics Research Section A 518 (2004) 106. http://dx.doi.org/10.1016/j.nima.2003.10.035.
[5] S. Aune, et al., Nuclear Instruments and Methods in Physics Research Section A 604 (2009) 15. http://dx.doi.org/10.1016/j.nima.2009.01.210.
[6] N. Abgrall, et al., Nuclear Instruments and Methods in Physics Research Section A 637 (2011) 25. http://dx.doi.org/10.1016/j.nima.2011.02.036.
[7] D. Abbaneo, et al., Nuclear Instruments and Methods in Physics Research Section A 718 (2013) 383. http://dx.doi.org/10.1016/j.nima.2012.10.058.
[8] P. Gasik, Journal of Instrumentation 9 (2014) C04035. http://dx.doi.org/10.1088/1748-0221/9/04/C04035.
[9] M. Iodice, Journal of Instrumentation 9 (2014) C01017. http://dx.doi.org/10.1088/1748-0221/9/01/C01017.
[10] M.A. Vos, Nuclear Instruments and Methods in Physics Research Section A 596 (2008) 29. http://dx.doi.org/10.1016/j.nima.2008.07.129.
[11] S. Gales, Progress in Particle and Nuclear Physics 59 (2007) 22. http://dx.doi.org/10.1016/j.ppnp.2006.12.021.
[12] H. Sakurai, Nuclear Physics A 805 (2008) 526c. http://dx.doi.org/10.1016/j.nuclphysa.2008.02.291.
[13] D. Leitner, et al., in: Proceedings of SRF2011, Chicago, USA, 2011.
[14] R. York, et al., in: Proceedings of LINAC2010, Tsukuba, Japan, 2010.
[15] B. Blank, et al., Nuclear Instruments and Methods in Physics Research Section A 613 (2010) 65. http://dx.doi.org/10.1016/j.nima.2009.10.140.
[16] A.A. Vorobyov, et al., Nuclear Instruments and Methods in Physics Research Section A 270 (1988) 419. http://dx.doi.org/10.1016/0168-9002(88)90710-3.
[17] A. Hashimoto, et al., Nuclear Instruments and Methods in Physics Research Section A 556 (2006) 339. http://dx.doi.org/10.1016/j.nima.2005.10.018.
[18] C.E. Demonchy, et al., Nuclear Instruments and Methods in Physics Research Section A 583 (2007) 341. http://dx.doi.org/10.1016/j.nima.2007.09.022.
[19] J. Pancin, et al., Nuclear Instruments and Methods in Physics Research Section A 735 (2014) 532. http://dx.doi.org/10.1016/j.nima.2013.09.068.
[20] D. Suzuki, et al., Nuclear Instruments and Methods in Physics Research Section A 691 (2012) 39. http://dx.doi.org/10.1016/j.nima.2012.06.050.
[21] R. Akimoto, et al., in: Nuclear Science Symposium Conference Record (NSS/MIC), Knoxville, TN, USA, 2010, p. 1881. http://dx.doi.org/10.1109/NSSMIC.2010.5874101.
[22] J.P. Sephton, M.J.L. Turner, J.W. Leake, Nuclear Instruments and Methods in Physics Research 219 (1984) 534. http://dx.doi.org/10.1016/0167-5087(84)90227-8.
[23] M. Kobayashi, Nuclear Instruments and Methods in Physics Research Section A 562 (2006) 136. http://dx.doi.org/10.1016/j.nima.2006.03.001.
[24] T. Zerguerras, et al., Nuclear Instruments and Methods in Physics Research Section A 608 (2009) 397. http://dx.doi.org/10.1016/j.nima.2009.07.015.
[25] ⟨http://www.spectra-physics.com⟩.
[26] ⟨http://www.industrialnetting.com⟩.
[27] J.-C. Santiard, et al., Gasplex A Low-Noise Analogue Signal Processor for Read Out of Gaseous Detectors, CERN-ECP/94-17.
[28] ⟨http://www.cremat.com⟩.
[29] ⟨http://www.caen.it⟩.
[30] ⟨http://www.photonis.com⟩.
[31] ⟨http://www.airliquide.com⟩.
[32] ⟨http://www.brooksinstrument.com⟩.
[33] B. Lombos, P. Sauvageau, C. Sandorfy, Chemical Physics Letters 1 (1967) 221. http://dx.doi.org/10.1016/0009-2614(67)85056-5.
[34] D. Thers, et al., Nuclear Instruments and Methods in Physics Research Section A 469 (2001) 133. http://dx.doi.org/10.1016/S0168-9002(01)00769-0.
[35] F. Penning, Zeitschrift für Physik 46 (1928) 335.
[36] F. Penning, Physica 1 (1934) 1028.
[37] ⟨http://physics.nist.gov/PhysRevData/ASD/levels_form.html⟩.
[38] ⟨http://physics.nist.gov/PhysRevData/ASD/lines_form.html⟩.
[39] H. Schindler, S.F. Biagi, R. Veenhof, Nuclear Instruments and Methods in Physics Research Section A 624 (2010) 78. http://dx.doi.org/10.1016/j.nima.2010.09.072.
[40] S.F. Biagi, Nuclear Instruments and Methods in Physics Research Section A 421 (1999) 234. http://dx.doi.org/10.1016/S0168-9002(98)01233-9.
[41] J. Derré, et al., Nuclear Instruments and Methods in Physics Research Section A 449 (2000) 314. http://dx.doi.org/10.1016/S0168-9002(99)01452-7.
[42] J.A. Mir, et al., IEEE Transactions on Nuclear Science NS-55 (2008) 2334. http://dx.doi.org/10.1109/TNS.2008.2001887.

[43] J. Vavr'a, A. Sharma, Nuclear Instruments and Methods in Physics Research Section A 478 (2002) 235. http://dx.doi.org/10.1016/S0168-9002(01)01763-6.
[44] R. Bellazzini, et al., Nuclear Instruments and Methods in Physics Research Section A 581 (2007) 246. http://dx.doi.org/10.1016/j.nima.2007.07.098.
[45] G.F. Knoll, Radiation Detection and Measurements, 2nd ed., Wiley and Sons, New-York, USA (1989) 175–176.
[46] W. Legler, Zeitschrift für Naturforschung 16a (1961) 253.
[47] R. Veenhof, Nuclear Instruments and Methods in Physics Research Section A 419 (1998) 726. http://dx.doi.org/10.1016/S0168-9002(98)00851-1.
[48] G.D. Alkhazov, Nuclear Instruments and Methods in Physics Research 89 (1970) 155. http://dx.doi.org/10.1016/0029-554X(70)90818-9.